


Dynamics of polydisperse multiple emulsions in microfluidic channelsA. Tiribocchi ^{1,*}, A. Montessori,¹ M. Durve,² F. Bonaccorso,^{1,2,3} M. Lauricella,¹ and S. Succi^{1,2,4}¹*Istituto per le Applicazioni del Calcolo CNR, via dei Taurini 19, 00185 Rome, Italy*²*Center for Life Nano Science@La Sapienza, Istituto Italiano di Tecnologia, 00161 Roma, Italy*³*Department of Physics and INFN, University of Rome "Tor Vergata," Via della Ricerca Scientifica, 00133 Rome, Italy*⁴*Institute for Applied Computational Science, John A. Paulson School of Engineering and Applied Sciences, Harvard University, Cambridge, Massachusetts 02138, USA*

(Received 21 October 2021; accepted 9 December 2021; published 27 December 2021)

Multiple emulsions are a class of soft fluid in which small drops are immersed within a larger one and stabilized over long periods of time by a surfactant. We recently showed that, if a *monodisperse* multiple emulsion is subject to a pressure-driven flow, a wide variety of nonequilibrium steady states emerges at late times, whose dynamics relies on a complex interplay between hydrodynamic interactions and multibody collisions among internal drops. In this work, we use lattice Boltzmann simulations to study the dynamics of *polydisperse* double emulsions driven by a Poiseuille flow within a microfluidic channel. Our results show that their behavior is critically affected by multiple factors, such as initial position, polydispersity index, and area fraction occupied within the emulsion. While at low area fraction inner drops may exhibit either a periodic rotational motion (at low polydispersity) or arrange into nonmotile configurations (at high polydispersity) located far from each other, at larger values of area fraction they remain in tight contact and move unidirectionally. This decisively conditions their close-range dynamics, quantitatively assessed through a time-efficiency-like factor. Simulations also unveil the key role played by the capsule, whose shape changes can favor the formation of a selected number of nonequilibrium states in which both motile and nonmotile configurations are found.

DOI: [10.1103/PhysRevE.104.065112](https://doi.org/10.1103/PhysRevE.104.065112)**I. INTRODUCTION**

Dazzling examples of hierarchical soft materials, i.e., organized states of matter made of multilength scale units [1], are ubiquitous in nature. They include bones [2], DNA [3], and cells [4], as well as liquid crystals [5], mesoporous materials [6], bijels [7], and foams [8,9], to name but a few. Of particular relevance to us are multiple emulsions, a pristine compartmentalized soft fluid made of distinct immiscible drops (often termed as cores, of size up to 100 μm) encapsulated within a larger one and stabilized through a surfactant adsorbed onto their interface [10–14].

Due to their fascinating architectural design encompassing various lengthscales (from the interface of a few nanometers to the diameter of the outer drop of hundreds of micrometers), these materials have found applications in disparate sectors of modern industry, such as pharmaceuticals in drug delivery [15–17], cosmetics in personal care items [18,19], food science in low-calorie products [20–23], and tissue engineering [24–27]. Intriguingly, they recently served as a platform to study cell-cell and cell-bacteria interactions enclosed in a capsule flowing within capillaries [26,28–30].

Multiple emulsions are usually manufactured within microfluidic channels, such as T-junctions and flow-focusing devices [14], by means of a single or two-step emulsification process [13,31–33], techniques generally guaranteeing a large production rate combined with an ordered

design [11,34–36], in which the degree of monodispersity is much higher than that accessible using conventional homogenizers, such as shear mixers [37]. Their mechanical properties can be modulated by properly tuning a number of key physical parameters, such as viscosity of the middle fluid to harden or jelly the capsule, surface tension of the drops to modify their shape, the amount and type of surfactant solution to prevent coalescence, as well as the degree of polydispersity [10,38,39]. The latter, in particular, can be decisively affected by the hydrodynamic forces mediated by the thin film of fluid separating the cores, whose mechanical stability relies on a delicate balance between surface tension and disjoining pressure [40–42]. Such a balance is especially relevant when the emulsion is subjected to an external forcing, such as shear or Poiseuille flow, which is a common situation in microfluidic experiments. Indeed, hydrodynamics may foster collisions among cores when flowing within the microchannel, thus favoring shape deformations that can potentially lead to their breakups and merging [43–46]. Such effects would permanently alter the grain size of the cores and ultimately modify their rate of polydispersity, eventually jeopardizing the homogeneity of the material, a feature often required, for example, in the design of soft porous matrices, such as tissue scaffold [27]. In addition, polydisperse cores may also be produced upstream due to an uncontrolled breakup of the dispersed fluid at the orifice located at the injection channel [47]. It is thus crucial to understand how hydrodynamics and polydispersity affect the mechanics of a multiple emulsion under flow, in particular the motion of the internal cores and the morphology of the droplets.

*Corresponding author: a.tiribocchi@iac.cnr.it; adrianotiribocchi@gmail.com

In this work, we use lattice Boltzmann (LB) simulations [48] to study the dynamics of polydisperse multiple emulsions subject to a Poiseuille flow within a microfluidic channel. A number of relatively recent numerical works have been dedicated to model such physics either considering double emulsions (containing a single core) [49–56] or multiple emulsions with distinct monodisperse cores [57,58]. In the latter context, we have recently shown that a surprisingly wide variety of nonequilibrium steady states can potentially be found when these systems are subject to a pressure-driven flow [58]. They essentially range from states where the cores exhibit a persistent periodic motion, triggered by a dipolar fluid vortex formed within the shell, to further states in which the cores display a chaoticlike dynamics due to the complex interplay between many-body collisions and hydrodynamic interactions. Here, we take one step forward and show that a wider scenario emerges when considering a polydisperse mixture of drops confined within a fluid capsule. Our multiple emulsion consists of two drops of radii R_1 and R_2 with $R_2 > R_1$ and polydispersity index $h = R_2/R_1$ (see Fig. 1), immersed within a larger droplet. Their physics is captured by a multiphase field model [59,60], where the dynamics of a set of scalar fields accounting for the density of each droplet obeys a Cahn-Hilliard equation, while that of a vector field representing the fluid velocity is governed by the Navier-Stokes equation.

Our LB simulations show that the emulsion dynamics depends, in a nontrivial way, on a set of key physical parameters, such as the polydispersity of the cores and their initial position as well as the area fraction A_f that they occupy and the morphology of the capsule. At low values of A_f , for example, the cores may either exhibit a permanent periodic motion confined within half of the emulsion for long periods of time (for low h), or they might get stuck separately at the front or at the rear of the emulsion (for high h), in particular when the large core precedes the small one at the onset of the motion (once the Poiseuille flow is turned on). At high values of A_f , the cores arrange in nonmotile configurations remaining either far from each other or in close contact confined at the leading edge of the capsule, a behavior generally observed for higher values of h and regardless of their initial position. This range of dynamic behaviors importantly affects the interaction between the cores, a quantity evaluated in terms of a dimensionless number gauging the time spent by the drops in close contact during a simulation. Finally, we also show that modifications of the shape of the capsule can foster a range of nonequilibrium steady states partially akin to the ones mentioned earlier.

This paper is structured as follows. In Sec. II, we outline the thermodynamic properties of the emulsion and the numerical method. An approximate mapping with physical parameters is also provided. Section III is dedicated to a discussion of the physics at the steady state, in particular the structure of the velocity field and the behavior of the internal cores. This is assessed in terms of their initial position, the area fraction occupied in the emulsion, the polydispersity index, and the time spent in close contact. We also illustrate the role played by the shell in driving the motion of the cores through changes of its shape. In conclusion, some remarks close the paper.

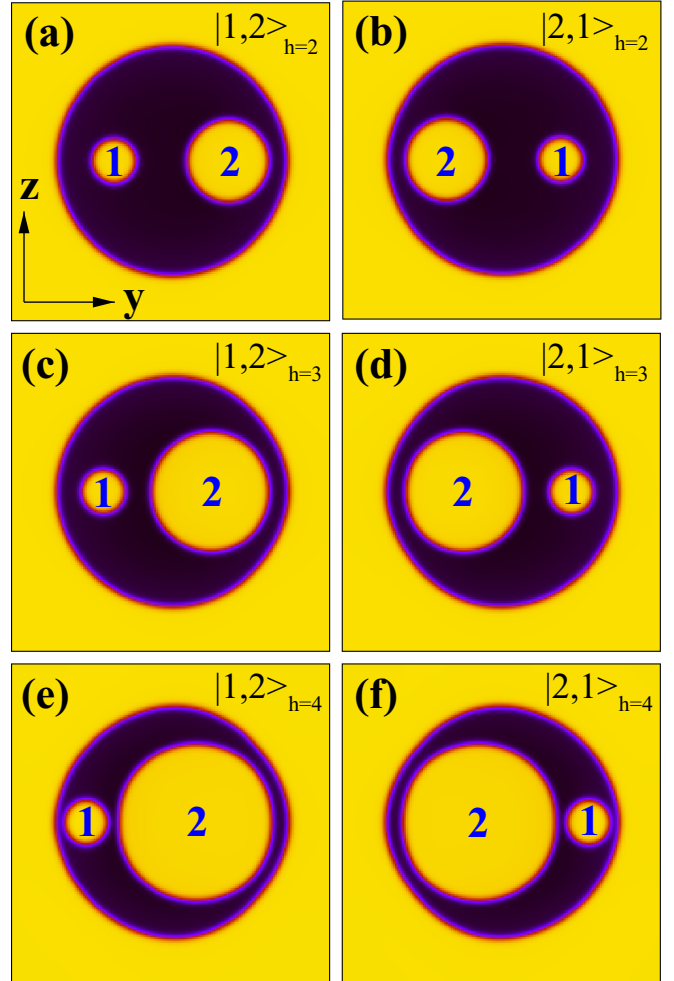


FIG. 1. Equilibrium configurations of three double emulsions with different sizes of the inner drops. (a), (b) $R_1 = 10$, $R_2 = 20$ ($h = 2$, $A_f \simeq 0.14$); (c), (d) $R_1 = 10$, $R_2 = 30$ ($h = 3$, $A_f \simeq 0.28$); and (e), (f) $R_1 = 10$, $R_2 = 40$ ($h = 4$, $A_f \simeq 0.47$). Only a portion of the microchannel is shown. Symbol $|i, j\rangle_{h=n}$ (where i, j, n are integer numbers) indicates a state in which two cores (such as 1 and 2) of different size are positioned next to each other, while h is the polydispersity index. Snapshots with equal values of h [such as (a) and (b), (c) and (d), (e) and (f)] only differ for the initial position of the cores. The radius of the external droplet has been kept fixed to $R_e = 60$. Colors represent the values of the order parameter ϕ , ranging from 0 (black) to $\simeq 2$ (yellow). This applies to all figures.

II. METHOD

A. Equations of motion

As in previous works [58,60–63], we use a multiphase field approach fully incorporating hydrodynamic interactions to model the physics of a multicore emulsion. Basically, a set of scalar fields $\phi_i(\mathbf{r}, t)$, $i = 1, \dots, N$ (where N is the total number of droplets) accounts for the density of each droplet at position \mathbf{r} and time t , while a vector field $\mathbf{v}(\mathbf{r}, t)$ describes the fluid velocity.

Each phase field ϕ_i obeys an advection-diffusion equation

$$D_t \phi_i = M \nabla^2 \mu_i, \quad (1)$$

where $D_t = \frac{\partial}{\partial t} + \mathbf{v} \cdot \nabla$ is the material derivative, M is the mobility, and μ_i is the chemical potential of the i th droplet.

The time evolution of fluid velocity $\mathbf{v}(\mathbf{r}, t)$ is governed by the Navier-Stokes equation, which, in the incompressible limit, reads

$$\rho \left(\frac{\partial}{\partial t} + \mathbf{v} \cdot \nabla \right) \mathbf{v} = -\nabla p + \eta \nabla^2 \mathbf{v} - \sum_i \phi_i \nabla \mu_i. \quad (2)$$

Here p is the hydrodynamic pressure and η is the dynamic viscosity.

Finally, the chemical potential appearing in Eqs. (1) and (2) is defined as $\mu_i \equiv \frac{\delta \mathcal{F}}{\delta \phi_i}$, where $\mathcal{F} = \int f d^3 \mathbf{r}$ is the free energy encoding the equilibrium properties of the mixture [64,65]. Its density f is given by

$$f = \sum_i^N \left(\frac{a}{4} \phi_i^2 (\phi_i - \phi_0)^2 + \frac{k}{2} (\nabla \phi_i)^2 \right) + \sum_{i,j,i < j} \epsilon \phi_i \phi_j, \quad (3)$$

where the first two terms ensure the existence of two minima, $\phi_i = \phi_0$ (with $\phi_0 \simeq 2$) inside the i th droplet and $\phi_i = 0$ outside, separated by a fluid interface. These two contributions also determine the surface tension $\sigma = \sqrt{8ak/9}$ and the interfacial thickness $\xi = 2\sqrt{2k/a}$ [66,67], in which a and k are positive constants. Finally, the last term of Eq. (3) represents a repulsive potential of strength ϵ , mimicking the effects produced, at the mesoscale level, by a surfactant adsorbed onto the droplet interfaces.

B. Numerical aspects

Equations (1) and (2) are numerically solved by means of a hybrid LB method [48,66,68,69], in which the advection-relaxation equations are integrated via a finite-difference Euler algorithm while the Navier-Stokes equation is integrated through a predictor-corrector LB scheme [70–73].

Simulations are run on two-dimensional rectangular lattices of size $L_y = 800$ (horizontal) and $L_z = 170$ (vertical). Periodic boundary conditions are set along the y -direction, while two parallel flat walls are placed at $z = 0$ and $z = L_z$. Here no-slip conditions hold for the velocity field \mathbf{v} , meaning that $v_z(z = 0, z = L_z) = 0$, while neutral wetting holds for the fields ϕ_i . The latter ensures that mass flux through the walls is absent (i.e., $\mathbf{n} \cdot \nabla \mu_i|_{z=0, z=L_z} = 0$, where \mathbf{n} is a unit vector normal the boundaries), and interfaces are perpendicular to the walls [i.e., $\mathbf{n} \cdot \nabla (\nabla^2 \phi_i)|_{z=0, z=L_z} = 0$].

In Fig. 1 we show three examples of double emulsions with different polydispersity index $h = R_2/R_1$, where R_1 and R_2 are the radii of cores 1 (small) and 2 (large), respectively. Emulsions with equal values of h [such as (a) and (b), (c) and (d), (e), and (f)] are prepared in two initial states, differing in the initial position of the cores. In Fig. 1(a), for example, core 1 with radius $R_1 = 10$ lattice sites is located on the left side of core 2 having radius $R_2 = 20$, while the radius of the external droplet is $R_e = 60$. This value, kept fixed in the simulations, ensures that contacts between walls and emulsion are minimized. In Fig. 1(b) the small core is positioned on the right side of the large one. Hence in both cases one has $h = 2$ and an area fraction occupied by the cores equal to $A_f = \frac{\pi \sum_i R_i^2}{\pi R_e^2} \simeq 0.14$. Such states are indicated as $|1, 2\rangle_{h=2}$

[Fig. 1(a)] and $|2, 1\rangle_{h=2}$ [Fig. 1(b)]. In Figs. 1(c) and 1(d), one has $R_1 = 10$ and $R_2 = 30$ ($h = 3$, $A_f \simeq 0.28$), and in Figs. 1(e) and 1(f), $R_1 = 10$ and $R_2 = 40$ ($h = 4$, $A_f \simeq 0.47$). Since three drops are considered (two cores and the shell), one needs three phase fields. In particular, the fields ϕ_1 and ϕ_2 refer to droplets 1 and 2, and they are positive (equal to $\simeq 2$) within each drop and zero everywhere else. The field ϕ_3 of the external droplet is positive outside and zero elsewhere. Once the droplets are relaxed toward a near-equilibrium state, a pressure gradient Δp is applied to produce a Poiseuille flow. This is modeled through the inclusion of a body force pushing the emulsion rightwards, along the positive y axis.

If not stated otherwise, following previous works [58] the thermodynamic parameters have been chosen as follows: $a = 0.07$, $k = 0.1$, $M = 0.1$, $\eta = 1.67$, $0.01 < A_f < 0.5$, $\Delta x = 1$ (mesh step), $\Delta t = 1$ (time step), and $\epsilon = 0.05$. In particular, the values of the parameters a and k fix the surface tension $\sigma \simeq 0.08$ and the interfacial width $\xi \simeq 3.5$, while the diffusion constant is $D = \text{Ma} = 0.007$. Finally, the value of ϵ is sufficiently high to prevent droplet merging.

A mapping between these simulation parameters and real values can be built by fixing the typical length, time, and force scale as $L = 1 \mu\text{m}$, $T = 10 \mu\text{s}$, and $F = 10 \text{ nN}$, respectively (in simulation units, these scales are all equal to 1). Hence this corresponds to a microfluidic channel of length $\sim 1 \text{ mm}$ in which droplets of diameter ranging from $\sim 10 \mu\text{m}$ (cores) to $\sim 100 \mu\text{m}$ (shell) have a surface tension of 1 mN/m and are immersed in a fluid of viscosity $\eta \simeq 10^{-1} \text{ Pa s}$ (equal viscosity is assumed for the fluid inside and outside the droplets). The Reynolds number, defined as $\text{Re} = \frac{\rho D_e v_{\text{max}}}{\eta}$, where v_{max} is the maximum speed in the channel and D_e is the diameter of the shell, varies roughly between 0.5 ($v_{\text{max}} \simeq 0.007$, $\Delta p = 3 \times 10^{-4}$) and 5 ($v_{\text{max}} \simeq 0.025$, $\Delta p = 10^{-3}$), while the capillary number $\text{Ca} = \frac{v_{\text{max}} \eta}{\sigma}$ ranges from 0.1 to 1 .

With these numbers, gravity effects can be neglected since assuming $\Delta \rho / \rho_w = (\rho_w - \rho_o) / \rho_w \sim 0.1$ (where the water density $\rho_w = 10^3 \text{ Kg/m}^3$ and a typical oil density $\rho_o \sim 9 \times 10^2 \text{ Kg/m}^3$), one has a Bond number $\text{Bo} = \Delta \rho g R^2 / \sigma \sim 10^{-2} - 10^{-3}$, where g is the gravity acceleration.

III. RESULTS

We start by describing steady states and shape deformations observed when a two-core emulsion, with a different polydispersity ratio, is subject to a Poiseuille flow. Afterwards we focus on the contact dynamics among cores observed at different values of A_f , and finally we elucidate the role played by the shape of the shell in selecting specific steady states.

A. Steady-state shapes and core dynamics

Starting from the set of equilibrated configurations shown in Fig. 1, we impose a Poiseuille flow that pushes the multi-core emulsion along the positive y axis, i.e., the longitudinal direction of the microchannel. Once the flow is switched on, the shell progressively stretches while the internal cores are dragged towards its front. In these conditions, the fluid velocity exhibits two well-defined counter-rotating vortices within the emulsion significantly affecting the dynamics of the internal cores [58].

If $h = 2$, for example, one may observe two distinct scenarios, whose evolution depends crucially on the way the emulsion is initially prepared. In the first one, observed starting from the state $|1, 2\rangle_{h=2}$, both cores accumulate at the leading edge of the shell and only temporarily arrange in a row. Indeed, such a configuration is unstable to weak perturbations of the flow, an effect due to the coupling between the velocity field and the fluid interfaces [58]. This leads to a state in which the large core remains stuck at the front of the emulsion while the small one initially shifts upwards and then is dragged backward until its motion relative to the shell ceases [see movie M1 [74], Fig. 2(a)]. Following an analogous mechanism, the small core may alternatively shift downwards, remaining confined within the lower sector of the emulsion, a condition achieved by slightly diminishing Reynolds and capillary numbers [58]. In both cases, at late times the cores and the shell move unidirectionally rightwards and no further changes are observed in their trajectories [see Figs. 3(a) and 3(b), where the displacement $\Delta \mathbf{r}_{cm}$ of the cores with respect to the shell is plotted over time]. In the second scenario obtained starting from the state $|2, 1\rangle_{h=2}$, once the rowlike arrangement of the cores at the front of the shell is destabilized, the large core is initially driven backwards by the upper vortex, but, unlike the previous case, it is followed by the small one. They move together backwards and then forward, exhibiting a persistent periodic motion along an almost circular trajectory confined within the upper region of the emulsion [see movie M2 [74], Fig. 2(b), and Figs. 3(a) and 3(b)]. Here too, decreasing Re and Ca leads to a state where both cores display the periodic motion within the lower part of the emulsion. We note incidentally that one may also initially align the centers of mass of the cores along the z direction rather than the midline. If such conditions are set, under Poiseuille flow the cores are essentially driven forward by the fluid, remaining confined within the regions (upper or lower) selected from scratch. These results are in agreement with the ones discussed in Ref. [58], where the dynamics of a *monodisperse* multicore emulsion under Poiseuille flow has been studied.

If $h = 3$, the dynamic behavior is overall simpler, although, once again, it is importantly affected by the initial arrangement of the cores. We basically find that, starting from the state $|1, 2\rangle_{h=3}$, at late times the drops attain a steady configuration [see Fig. 2(c) and movie M3 [74]] akin to that observed in Fig. 2(a), whereas starting from the state $|2, 1\rangle_{h=3}$, both cores accumulate at the front of the emulsion where they stick [see Fig. 2(d) and movie M4 [74]]. The latter occurs because the large core initially follows the small one once the Poiseuille flow is turned on. Then it approaches and entraps core 1 at the front of the emulsion, in a region where the effect of the fluid vortices is too weak to destabilize the suspension. In both cases (c) and (d), at the steady state the cores move unidirectionally at constant speed without displaying any considerable deviation from their path [see also Figs. 3(c) and 3(d)]. Note incidentally that besides the two fluid recirculations formed within the shell (the black region), two further vortices appear in the large core (highlighted by magenta arrows), counter-rotating with respect to the contiguous one due to the continuity of the field at the interface. Such structures look seemingly absent in smaller drops [such as core 1 in

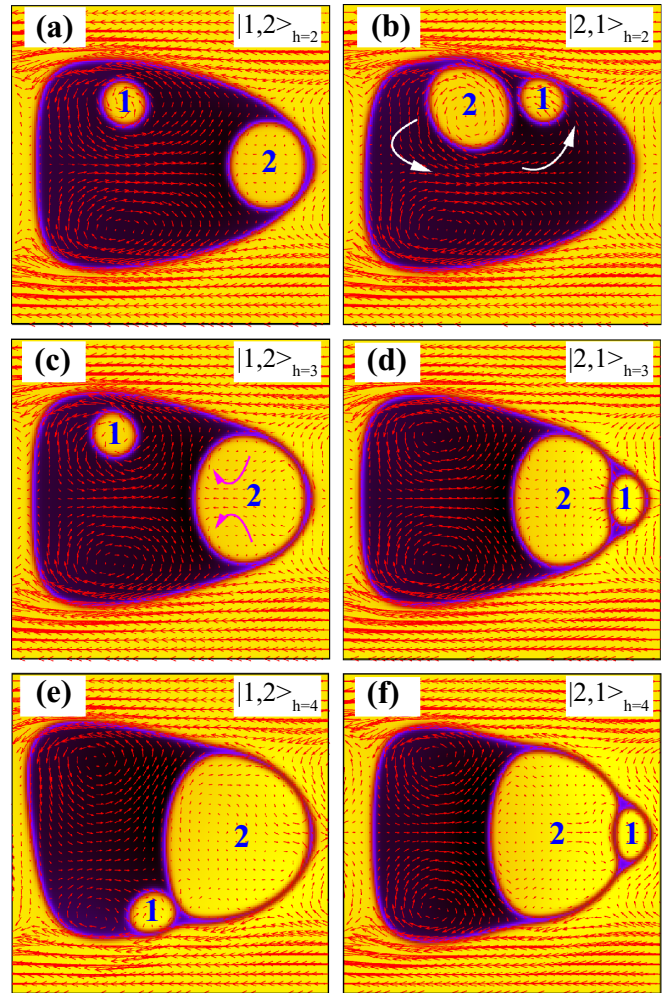


FIG. 2. Nonequilibrium steady states observed in polydisperse two-core emulsions subject to a Poiseuille flow. Here $Re \simeq 2$ and $Ca \simeq 0.53$. The left column represents states whose initial conditions shown in Figs. 1(a), 1(c), and 1(e) are of the form $|1, 2\rangle_{h=2,3,4}$, while the right column stems from initial configurations of the form $|2, 1\rangle_{h=2,3,4}$. Red arrows indicate the velocity field computed in the frame of reference of the external droplet. If $h = 2$ (a), (b) one can identify two regimes: (i) one in which the large core gets stuck at the leading edge of the emulsion while the small one is captured by the upper fluid vortex, and (ii) a further one in which the cores exhibit a periodic motion triggered by the fluid vortex. In both cases, the whole emulsion is dragged rightwards by the flow. White arrows indicate the direction of motion of the cores. If $h = 3$ (c), (d) and $h = 4$ (e), (f), internal drops attain a nonmotile configuration, either akin to that shown in (a) or consisting of two cores stuck at the front of the emulsion. Magenta arrows in (c) represent the direction of two counterclockwise vortices formed within the larger core.

Fig. 2(d)], very likely because of a lack of sufficient resolution of the present mesoscale approach, which captures with very good accuracy fluid vortices whose typical size is generally comparable with that of the pertaining droplet (which is of the order of a few microns).

At increasing values h , such as $h = 4$ [see Figs. 2(e) and 2(f)], the steady states show analogous dynamic features to the ones observed for $h = 3$, except for the shape attained by the shell. Indeed, while at low values of h the exter-

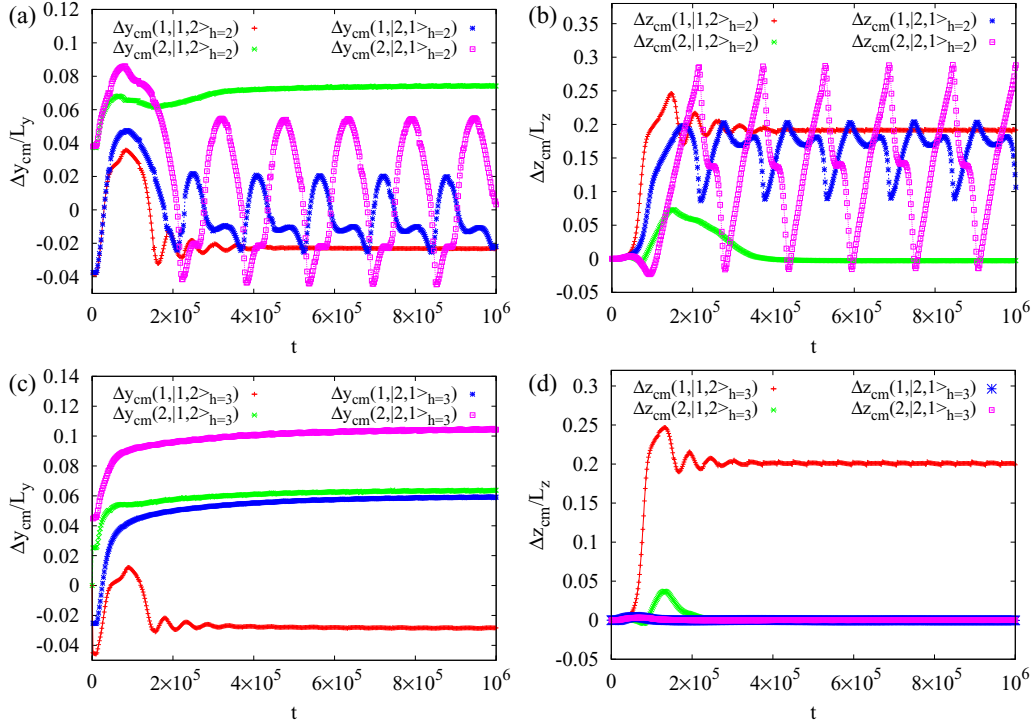


FIG. 3. Time evolution of the displacement Δy_{cm} (left column) and Δz_{cm} (right column) of the internal cores. The top panels refer to states of $|1, 2\rangle$ and $|2, 1\rangle$ with $h = 2$, while the bottom ones concern those with $h = 3$. If $h = 2$, cores may either get transported by the fluid and move unidirectionally, or they may display a persistent periodic motion confined within a region of the emulsion and triggered by the fluid vortex. If $h = 3$, the internal cores are generally dragged by the flow unidirectionally, either remaining sufficiently far from each other or accumulating at the front of the emulsion.

nal interface attains a rather well-defined bullet-shape profile [such as in Figs. 2(a) and 2(b)], for higher values it develops permanent local bulges at the front due to the close contact with the internal cores. The shape may, for instance, stretch along the flow direction [see Figs. 2(d) and 2(f)] or acquire a protuberance located at the top rear [see Fig. 2(e)], resulting from the asymmetry of the vortices induced by the small drop stuck in the lower region. The dynamics of the cores discussed in Fig. 2 qualitatively holds for decreasing values of Re and Ca as well. Setting $Re \simeq 0.5$, $Ca \simeq 0.1$, and $h = 2$, for example, at the steady state the shell acquires a more rounded shape, a condition allowing the cores to escape from its front and migrate either downwards or upwards where they remain confined, exhibiting a dynamics akin to that shown in Fig. 2(b).

These results suggest that changing the polydispersity index could potentially suppress the internal motion of the cores (thus stabilizing the emulsion) and significantly affect their close contact dynamics, while only mildly altering the shape of the emulsion, which basically remains that of a projectile usually observed for droplets subject to a Poiseuille flow [58]. The next section will be dedicated to a quantitative assessment of the interaction of cores in terms of the time they spend in close contact.

B. Close-contact dynamics among cores

In a previous work [63] we showed that, when the polydispersity index increases, contacts among cores are favored

in multiple emulsions under shear flow. Assessing interactions and reciprocal distance may be relevant, for example, in microbiological experiments in which cells dispersed in an aqueous environment (like our cores encapsulated within the emulsion) come in contact with pathogenic bacteria causing human disease [29].

The close-contact dynamics can be approximately evaluated by comparing the reciprocal distance $|\Delta \mathbf{r}_{cm}| = |\mathbf{r}_{cm,1} - \mathbf{r}_{cm,2}|$ between the centers of mass of each core with the distance $d = R_1 + R_2 + l$, where R_1 and R_2 are the radii of the cores and l is the length of the thin film separating opposite interfaces in contact. Assuming a width of interface ξ approximately equal to four to five lattice sites, we set $l = 2\xi$. If $|\Delta \mathbf{r}_{cm}| < d$, the cores are considered at a sufficiently close distance to temporarily sustain the film of fluid, whereas if $|\Delta \mathbf{r}_{cm}| > d$ they are too far away and reciprocal interaction is negligible. This quantity provides a reasonable measurement of the interaction as long as the shape deformations of the cores do not significantly depart from a near-spherical one.

1. Dynamics at low values of A_f

In Figs. 4(a) and 4(b) we show the time evolution of $|\Delta \mathbf{r}_{cm}|$ for a multiple emulsion prepared either in an initial state of type $|1, 2\rangle$ (in which the smaller drop 1 is located on the left side of the larger one 2) or in a state of type $|2, 1\rangle$ (the other way round), with area fraction A_f occupied by the cores ranging between 0.14 ($h = 2$) and 0.2 ($h = 1.11$). If, for example, $h = 2$ ($R_1 = 10$ and $R_2 = 20$) one has $d = 40$, and

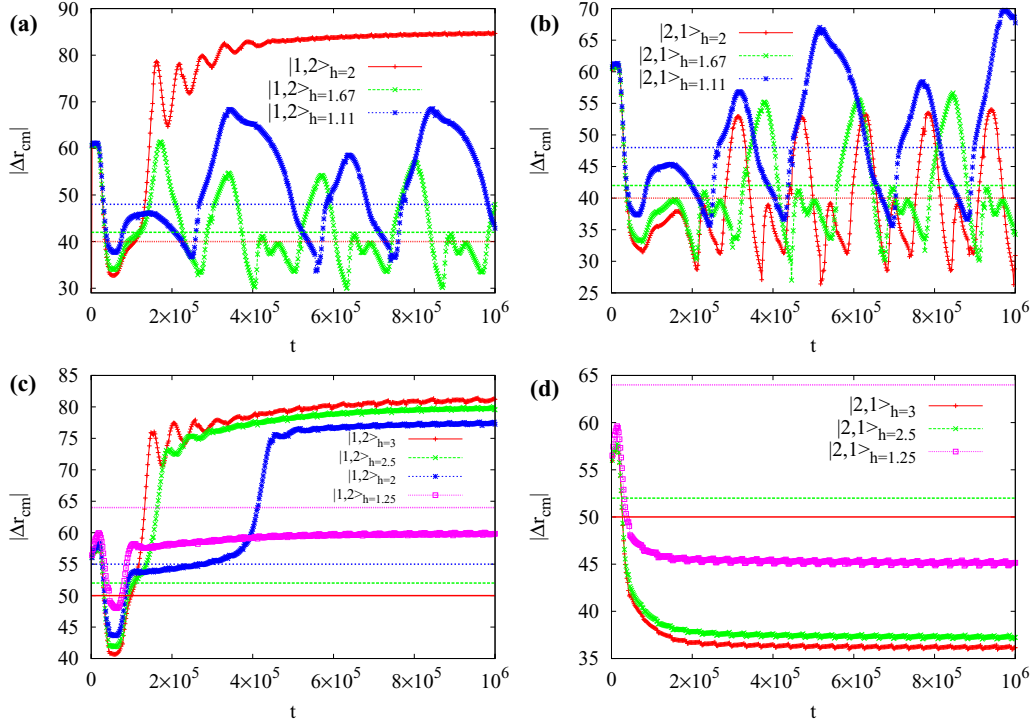


FIG. 4. Time evolution of the distance $|\Delta\mathbf{r}_{cm}|$ between the centers of mass of the cores, starting their motion from states of the type $|1, 2\rangle$ (a)–(c) and $|2, 1\rangle$ (b)–(d) and for different values of h . Horizontal lines indicate the distance $d = R_1 + R_2 + l$ below which cores interact, since opposite interfaces belonging to different drops sustain a temporary film of fluid. Assuming an interface width ξ approximately equal to four to five lattice sites, one has $l = 2\xi$. Thus in (a) and (b) $d = 40$ ($R_1 = 10$, $R_2 = 20$, $l = 10$) for $h = 2$ (red horizontal line), $d = 42$ ($R_1 = 12$, $R_2 = 20$, $l = 10$) for $h = 1.67$ (green horizontal line), and $d = 48$ ($R_1 = 18$, $R_2 = 20$, $l = 10$) for $h = 1.11$ (blue horizontal line). Note that here R_2 is fixed at 20 and R_1 increases. In (c) and (d) $d = 50$ ($R_1 = 10$, $R_2 = 30$, $l = 10$) for $h = 3$ (red horizontal line), $d = 52$ ($R_1 = 12$, $R_2 = 30$, $l = 10$) for $h = 2.5$ (green horizontal line), $d = 55$ ($R_1 = 15$, $R_2 = 30$, $l = 10$) for $h = 2$ (blue horizontal line), and $d = 64$ ($R_1 = 24$, $R_2 = 30$, $l = 10$) for $h = 1.25$ (purple horizontal line). Here R_2 is fixed at 30 and R_1 increases.

$|\Delta\mathbf{r}_{cm}|$ either attains a constant value higher than d [i.e., the cores remain sufficiently far from each other and collisions are negligible; see the red pluses in Fig. 4(a)] or it exhibits an oscillating behavior intersecting the horizontal line at $d = 40$ multiple times [see the red pluses in Fig. 4(b)]. The latter behavior essentially means that inner cores periodically come close ($\Delta\mathbf{r}_{cm} < d$) and detach ($\Delta\mathbf{r}_{cm} > d$) from early times onward. For decreasing values of h , the size of the cores approaches the monodisperse limit, a condition achieved by augmenting the radius of the smaller drop 1 while keeping constant that of the larger one 2. In these cases ($h = 1.67$ and 1.11, green crosses and blue asterisks, respectively), once again the cores display a persistent circular motion triggered by the fluid vortex, and they come in close contact multiple times. Their reciprocal distance shows a rather regular oscillating pattern once the steady state is attained (at approximately $t = 2 \times 10^5$ time steps), remaining below the interaction distance for long periods of time. In the next section, we will show that, unlike the physics just discussed, at higher values of A_f the contact dynamics is significantly different, despite the fact that the values of h will be akin to the ones considered so far.

2. Dynamics at intermediate values of A_f

In Figs. 4(c) and 4(d) we show the time evolution of $|\Delta\mathbf{r}_{cm}|$ for a multiple emulsion prepared either in a state $|1, 2\rangle$ (c) or $|2, 1\rangle$ (d) in which A_f ranges from 0.28 ($h = 3$, $R_1 = 10$, and $R_2 = 30$) to 0.41 ($h = 1.25$, $R_1 = 24$, and $R_2 = 30$). If $h = 3$, one has $d = 50$ and two opposite scenarios occur. Starting from a $|1, 2\rangle$ state, for instance, the cores come into contact only at early times, while afterwards they detach and remain separate [Fig. 4(c), red pluses], with the large drop stuck at the leading edge of the emulsion, and the small one in its bulk. In stark contrast, starting from a $|2, 1\rangle$ state, the two cores soon stick together and $|\Delta\mathbf{r}_{cm}|$ falls well below d for the entire simulation [Fig. 4(d), red pluses].

Note in particular that, unlike the cases discussed at low values of A_f , here for decreasing values of h the oscillating dynamics is replaced by a fully unidirectional motion, in which either the cores remain far apart for a large portion of time [Fig. 4(c), $h = 2.5$ and 2] or they stay in very close contact all the time [Fig. 4(c), $h = 1.25$ and Fig. 4(d), $h = 2.5$ and 1.25]. In Fig. 4(d), in particular, $|\Delta\mathbf{r}_{cm}|$ at late times is considerably below the corresponding value of d , an indication that inner drops are squeezed by the flow, and the distance between the centers of mass shortens significantly.

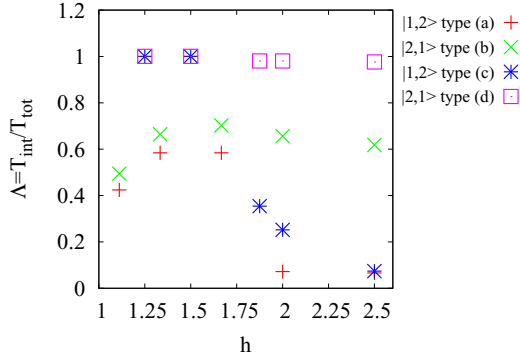


FIG. 5. Here we plot the ratio $\Lambda = T_{\text{int}}/T_{\text{tot}}$ for different values of h . The quantity T_{int} represents the time (in simulation units) in which two cores are in close contact and sustain a thin film of fluid, an effect occurring when $|\Delta \mathbf{r}_{cm}| < d$, while $T_{\text{tot}} = 10^6$ is the total simulation time. Note that in systems starting from a $|1, 2\rangle$ configuration [such as those in Figs. 1(a)–1(c) in which drop 1 is smaller than drop 2], the ratio $T_{\text{int}}/T_{\text{tot}}$ is high for low values of h (i.e., when drops have a comparable size and occupy a large portion of the emulsion) and diminishes as h increases (i.e., the size of droplet 1 lessens while that of drop 2 remains fixed). On the contrary, systems starting from a $|2, 1\rangle$ configuration display an approximately constant and high value of Λ .

3. Time efficiency factor

A more quantitative estimate of the effect of the polydispersity on the close contact dynamics can be gauged by introducing an efficiency-like parameter $\Lambda = T_{\text{int}}/T_{\text{tot}}$, defined as the ratio between the time T_{int} spent by the cores in close proximity (i.e., when $|\Delta \mathbf{r}_{cm}| < d$) and the total observation time T_{tot} (i.e., the simulation time, corresponding to 10^6 time steps). In Fig. 5 we show how Λ varies with h for double emulsions initially prepared in the state $|1, 2\rangle$ (red pluses and blue asterisks) and in the state $|2, 1\rangle$ (green crosses and magenta squares). In all cases, h is varied by changing the radius of the small drop (say, 1) and keeping fixed that of the large one (say, 2). Thus, for example, the plot $|1, 2\rangle$ type (a) is obtained by starting from a configuration like the one shown in Fig. 1(a) and by either decreasing or increasing the radius of drop 1. This changes h from 1.25 ($R_1 = 16, R_2 = 20$) to 2.5 ($R_1 = 8, R_2 = 20$). An analogous scheme is used for the other plots.

Our results prove, once again, that Λ is critically affected by (i) the initial position of the cores, and (ii) the area fraction they occupy. Indeed, considering the states $|1, 2\rangle$, Λ attains either intermediate or high values at low h (lower than 2), since the cores either remain stuck together or they exhibit an approximately circular motion in which they periodically approach each other and drift apart. At high h (larger than 2), Λ drastically reduces since the cores stay far away from each other. On the contrary, emulsions starting from a $|2, 1\rangle$ state generally show high values of Λ for all values of h explored, since either cores move periodically along a circular path or they squeeze together at the leading edge of the external interface. Note also that Λ is generally equal to or higher than 0.5 for low h , namely when the area fraction A_f becomes larger than $\simeq 0.15$ (i.e., the size of the small drop approaches

that of the large one), whereas Λ can decrease for higher h , since A_f diminishes and cores are more easily advected by the velocity field, thus they spend a shorter amount of time in contact.

It is finally worth observing that the behavior of Λ obtained for a multiple emulsion subject to a Couette-like flow (discussed in Ref. [63]) shows a marked difference from that observed in this paper. Indeed, while in the former Λ has a well-defined trend in which it typically augments for increasing values of h and essentially regardless of the initial conditions, in the presence of a Poiseuille flow the scenario is more complex since, beside the polydispersity, both the initial conditions and the area fraction ultimately affect the fate of the contact dynamics.

C. Shape of the capsule

Before concluding, we dedicate this last section to pinpointing the effect produced by the external shell on the motion of the internal cores. Indeed, although our results suggest that polydispersity has only a mild effect on the shape of the shell (as long as A_f remains lower than approximately 0.5, indeed the highest values considered in the present study), one may wonder whether shape modifications of the external interface could favor a predefined dynamic behavior of the cores. Besides a theoretical interest *per se*, the characterization of such shape changes holds a significant relevance in practical applications, such as in drug delivery, where, for example, the time release of the drug, usually stored within the cores [15], is expected to occur faster in regions of high shape deformations [56].

In Fig. 6 we show a selection of nonequilibrium steady states of a two-core emulsion with $h = 2$ initially prepared in a state $|1, 2\rangle$. Here Re is kept fixed to ~ 2.5 while Ca is varied between ~ 0.1 and ~ 2 by changing the surface tension σ of the external interface. Like in previous simulations, the emulsion is driven rightwards by a Poiseuille flow which, besides modifying the shape of the shell, drags the cores along the same direction. Once they approach the front of the external interface, their subsequent dynamic behavior is found to depend decisively on the shape of the emulsion. At high values of Ca [see Figs. 6(a) and 6(f)] the capsule acquires a highly squeezed projectile shape exhibiting a reentrant deformation made of two sharp symmetric bulges located at the rear. Such a structure considerably alters the typical pattern of the velocity field, which now displays two deeply stretched vortices rotating counterclockwise. In this configuration, both cores arrest their internal motion at the leading edge of the emulsion where they remain stuck. This is likely due to a lack of space sufficient to allow for their internal movement and, concurrently, to a “weak” coupling with the velocity field, which, in this state, is unable to trigger their motion. At decreasing Ca [see Figs. 6(b) and 6(c) and Figs. 6(g) and 6(h)], the two rear protuberances disappear and the shell attains a wider fingerlike structure. This allows for a temporary internal motion of the small cores, which are located either in the upper or the lower part of the emulsion at the steady state. Now two well-defined counter-rotating vortices form within the shell, although they are still not capable of generating a net internal motion. Further diminishing Ca [Figs. 6(d) and 6(e)

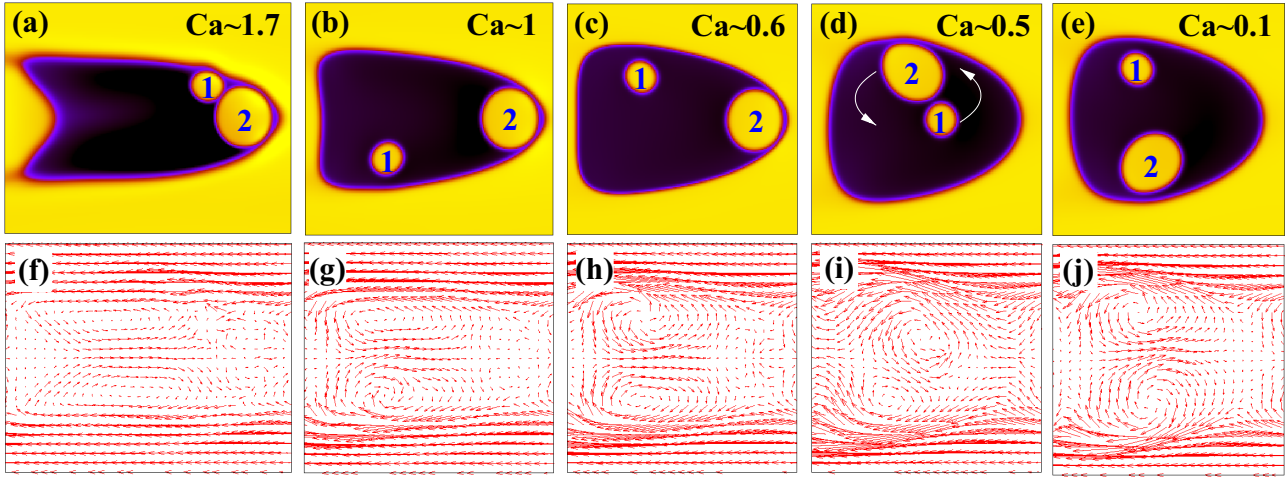


FIG. 6. The top row shows a selection of nonequilibrium steady states of a two-core emulsion with $h = 2$ (initially prepared in the state $|1, 2\rangle$) observed by varying the capillary number of the shell while keeping the Reynolds number fixed. At high values of Ca (a) the external droplet exhibits a highly squeezed projectilelike shape which essentially prevents the internal motion of the cores. Decreasing Ca (b), (c), the shell acquires a fingerlike configuration in which the cores separate and comove with the external droplet. Further diminishing Ca (d), (e), the shell takes on a rounded shape in which cores may either rotate periodically or migrate toward separate regions of the emulsion. The bottom row (f)–(j) shows the velocity field computed in the frame of reference of the shell.

and Figs. 6(i) and 6(j)], the capsule attains a large rounded shape at the steady state. Here the two symmetric vortices are wide enough to promote the motion of the cores, which either show a periodic dynamics (d) or remain trapped within two separate regions of the emulsion (e).

These results show that shape changes of the shell considerably modify the dynamics of the internal cores, thus further highlighting the multifaceted structure of the parameter phase space determining the fate of these systems, in stark contrast with the ones of the simple liquids they are made of (such as water and oil).

IV. CONCLUSIONS

To summarize, we have simulated, by using lattice Boltzmann methods, the dynamic behavior of a polydisperse multiple emulsion subject to a Poiseuille flow within a microfluidic channel, using a setup inspired to realistic laboratory experiments. To elucidate the physics, we have considered simple realizations of such emulsions, made of two cores of different size suspended within a larger drop. Despite the easy design, our results provide evidence of a complex scenario in which the properties of the mixture depend on a number of key features, such as the initial position and the area fraction occupied by the cores, as well as the polydispersity index and the shape of the surrounding shell.

At low area fraction (generally $A_f < 0.25$), for example, the cores may either display a persistent periodic motion confined within a region of the emulsion for low h (in agreement with previous studies [58]), or they may arrange into non-motile configurations, located far from each other, for high h . This behavior depends crucially on the way the emulsion is initially prepared, basically whether the large core precedes or follows the small one once the Poiseuille flow is turned on. At high area fraction, the cores remain firmly glued together

moving unidirectionally with the flow for low h , or they may also disconnect at high h .

Such dynamics also affects the time spent by the cores in contact, a phenomenon once again depending, in a nontrivial manner, on the aforementioned parameters. This effect has been assessed in terms of the ability of the cores to sustain a film of fluid formed between opposite interfaces during the motion, and it is quantitatively evaluated through the parameter Λ . In particular, we find that if the large core initially precedes the small one (state $|1, 2\rangle$), at low values of h , Λ ranges from 0.5 to 1, i.e., almost the entire simulation time. On the contrary, increasing h , Λ dramatically decreases since both cores are placed far apart and their interaction becomes negligible. If the large core follows the small one (state $|2, 1\rangle$), Λ remains considerably high regardless of the values of h , since the cores either periodically approach and separate or conjoin at the front the external interface. In addition, our findings suggest that the dynamics of the cores can be controlled by changes of capsule shape, ranging from a highly elongated structure observed at high values of Ca to an approximately circular one at low values of Ca . Their motion is guided by a typical double counter-rotating vortex which displays a considerably squeezed pattern at high Ca in contrast to a well-defined rounded motif at low Ca . It is worth mentioning that the mechanical properties of the emulsion can also be modified by releasing the approximation of equal viscosity between the dispersed, middle, and outer fluid adopted in this work. Increasing, for example, the viscosity of cores and shell is expected to harden the suspension and affect the structure of the velocity field [10], thus the dynamics of the cores as well. On the contrary, reducing their viscosity would gel the emulsion, likely favoring the breakup of the drops [75].

We finally note that the scenario described in this paper offers a perspective wider than that discussed in previous studies [58], in particular regarding the role played by the

polydispersity. Notwithstanding, several fundamental issues remain open. Delving, for example, into the physics of a multiple emulsion under flow when the volume fraction of the cores considerably overcomes the close packing fraction limit of hard spheres represents a challenging problem. Indeed, the encapsulation of a high packing fraction of drops requires a high control over a number of crucial parameters, such as the surface tension of the shell, the viscosity of the fluids involved, and the concentration of the surfactant solution [34,76]. This is fundamental to avoiding the effects that could potentially compromise the design, such as the rupture of the capsule (in the worst-case scenario) or the merging of the droplets, a phenomenon that would permanently alter the topological properties of the emulsion. Such physics is expected to be relevant, for instance, in a highly

packed multiple emulsion crossing a narrow constriction [39], where permanent shape deformations and memorylike effects result from the combined action of confinement and viscous dissipation. Understanding, for example, whether topological transitions (such as T1 events) occur mainly in the bulk or in the periphery of the emulsion is still an open problem, as well as determining whether a yield stress marks a transition from a solidlike to a fluid behavior [77].

ACKNOWLEDGMENTS

The authors acknowledge funding from the European Research Council under the European Union's Horizon 2020 Framework Programme (No. FP/2014-2020) ERC Grant Agreement No. 739964 (COPMAT).

-
- [1] R. Xu and Y. Xu, *Modern Inorganic Synthetic Chemistry* (Elsevier, Amsterdam, 2017).
- [2] U. Wegst, H. Bai, E. Saiz, A. P. Tomsia, and R. O. Ritchie, Bioinspired structural materials, *Nat. Mater.* **14**, 23 (2015).
- [3] D. Marenduzzo, *The Physics of DNA and Chromosomes* (IOP, Bristol, 2018).
- [4] D. Bray, *Cell Movements: From Molecules to Motility*, 2nd ed. (Garland, New York, 2000).
- [5] P. J. de Gennes and J. Prost, *The Physics of Liquid Crystals*, 2nd ed. (Oxford University Press, Oxford, 1993).
- [6] W. Li, J. Liu, and D. Zhao, Mesoporous materials for energy conversion and storage devices, *Nat. Rev. Mater.* **1**, 16023 (2016).
- [7] K. Stratford, J. Adhikari, I. Pagonabarraga, J. C. Desplat, and M. E. Cates, Colloidal jamming at interfaces: A route to fluid-bicontinuous gels, *Science* **309**, 2198 (2005).
- [8] D. J. Durian, Foam Mechanics at the Bubble Scale, *Phys. Rev. Lett.* **75**, 4780 (1995).
- [9] D. J. Durian, Bubble-scale model of foam mechanics: Melting, nonlinear behavior, and avalanches, *Phys. Rev. E* **55**, 1739 (1997).
- [10] A. S. Utada, E. L. Lorenceau, D. R. Link, P. D. Kaplan, H. A. Stone, and D. A. Weitz, Monodisperse double emulsions generated from a microcapillary device, *Science* **308**, 537 (2005).
- [11] A. R. Abate and D. A. Weitz, High-order multiple emulsions formed in poly(dimethylsiloxane) microfluidics, *Small* **5**, 2030 (2009).
- [12] S. S. Datta, A. Abbaspourrad, E. Amstad, J. Fan, S. H. Kim, M. Romanowsky, H. C. Shum, B. Sun, A. S. Utada, M. Windbergs, S. Zhou, and D. A. Weitz, 25th anniversary article: Double emulsion templated solid microcapsules: Mechanics and controlled release, *Adv. Mater.* **26**, 2205 (2014).
- [13] S. Ding, C. A. Serra, T. F. Vandamme, W. Yu, and N. Anton, Double emulsions prepared by two-step emulsification: History, state-of-the-art and perspective, *J. Controlled Release* **295**, 31 (2019).
- [14] G. T. Vladisavljevic, R. Al Nuamani, and S. A. Nabavi, Microfluidic production of multiple emulsions, *Micromachines* **8**, 75 (2017).
- [15] K. Pays, J. Giermanska-Kahn, B. Pouligny, J. Bibette, and F. Leal-Calderon, Double emulsions: How does release occur?, *J. Controlled Release* **79**, 193 (2002).
- [16] E. C. Sela, M. Chorny, N. Koroukhov, H. D. Danenberg, and G. Golomb, A new double emulsion solvent diffusion technique for encapsulating hydrophilic molecules in PLGA nanoparticles, *J. Controlled Release* **133**, 90 (2009).
- [17] A. S. Mao, B. Özkale, N. J. Shah, K. H. Vining, T. Descombes, L. Zhang, C. M. Tringides, S. W. Wong, J. W. Shin, D. T. Scadden, D. A. Weitz, and D. J. Mooney, Programmable microencapsulation for enhanced mesenchymal stem cell persistence and immunomodulation, *Proc. Natl. Acad. Sci. USA* **116**, 15392 (2019).
- [18] M.-H. Lee, S.-G. Oh, S.-K. Moon, and S.-Y. Bae, Preparation of silica particles encapsulating retinol using o/w/o multiple emulsions, *J. Colloid Interface Sci.* **240**, 83 (2001).
- [19] D.-H. Lee, Y.-M. Goh, J.-S. Kim, H.-K. Kim, H.-H. Kang, K.-D. Suh, and J.-W. Kim, Effective formation of silicone-in-fluorocarbon-in-water double emulsions: Studies on droplet morphology and stability, *J. Dispersion Sci. Technol.* **23**, 491 (2002).
- [20] E. Dickinson, Double emulsions stabilized by food biopolymers, *Food Biophys.* **6**, 1 (2011).
- [21] L. Sapei, M. A. Naqvi, and D. Rousseau, Stability and release properties of double emulsions for food applications, *Food Hydrocoll.* **27**, 316 (2012).
- [22] T. A. Comunian, A. Abbaspourrad, C. S. Favaro-Trindade, and D. A. Weitz, Fabrication of solid lipid microcapsules containing ascorbic acid using a microfluidic technique, *Food. Chem.* **152**, 271 (2014).
- [23] G. Muschiolik and E. Dickinson, Double emulsions relevant to food systems: Preparation, stability, and applications, *Comprehensive Rev. Food Sci. Food. Safety* **16**, 532 (2017).
- [24] F. G. Rocha, C. A. Sundback, N. J. Krebs, J. Kent Leach, D. J. Mooney, S. W. Ashley, J. P. Vacanti, and E. E. Whang, The effect of sustained delivery of vascular endothelial growth factor on angiogenesis in tissue-engineered intestine, *Biomaterials* **29**, 2884 (2008).
- [25] B. G. Chung, K. H. Lee, A. Khademhosseini, and S. H. Lee, Microfluidic fabrication of microengineered hydrogels and their application in tissue engineering, *Lab Chip* **12**, 45 (2012).
- [26] H. F. Chan, Y. Zhang, Y. P. Ho, Y. A. Chiu, Y. Jung, and K. W. Leong, Rapid formation of multicellular spheroids in double-emulsion droplets with controllable microenvironment, *Sci. Rep.* **3**, 3462 (2013).

- [27] M. Costantini, C. Colosi, J. Guzowski, A. Barbetta, J. Jaroszewicz, W. Swieszkowski, M. Dentini, and P. Garstecki, Highly ordered and tunable polyhypes by using microfluidics, *J. Mater. Chem. B* **2**, 2290 (2014).
- [28] Y. Zhang, H. P. Ho, Y. L. Chiu, H. F. Chan, B. Chlebina, T. Schuhmann, L. You, and K. W. Leong, A programmable microenvironment for cellular studies via microfluidics-generated double emulsions, *Biomaterials* **34**, 4564 (2013).
- [29] T. S. Kaminski, O. Scheler, and P. Garstecki, Droplet microfluidics for microbiology: Techniques, applications and challenges, *Lab Chip* **16**, 2168 (2016).
- [30] C.-H. Choi, H. Wang, H. Lee, J. H. Kim, L. Zhang, A. Mao, D. J. Mooney, and D. A. Weitz, One-step generation of cell-laden microgels using double emulsion drops with a sacrificial ultra-thin oil shell, *Lab Chip* **16**, 1549 (2016).
- [31] S.-H. Kim and D. A. Weitz, One-step emulsification of multiple concentric shells with capillary microfluidic devices, *Angew. Chem. Int. Ed.* **123**, 8890 (2011).
- [32] S. Kim, K. Kim, and S. Q. Choi, Controllable one-step double emulsion formation via phase inversion, *Soft Matter* **14**, 1094 (2018).
- [33] P. S. Clegg, J. W. Tavacoli, and P. J. Wilde, One-step production of multiple emulsions: Microfluidic, polymer-stabilized and particle-stabilized approaches, *Soft Matter* **12**, 998 (2016).
- [34] L. Y. Chu, A. S. Utada, R. K. Shah, J. W. Kim, and D. A. Weitz, Controllable monodisperse multiple emulsions, *Angew. Chem. Int. Ed.* **46**, 8970 (2007).
- [35] W. Wang, R. Xie, X. J. Ju, T. Luo, L. Liu, and D. A. Weitz, Controllable microfluidic production of multicomponent multiple emulsions, *Lab Chip* **11**, 1587 (2011).
- [36] H. C. Shum, J. Varnell, and D. A. Weitz, Microfluidic fabrication of water-in-water (w/w) jets and emulsions, *Biomicrofluidics* **6**, 012808 (2012).
- [37] D. J. McClemets, Advances in fabrication of emulsions with enhanced functionality using structural design principles, *Curr. Opin. Colloid Interface Sci.* **17**, 235 (2012).
- [38] A. Montessori, M. Lauricella, A. Tiribocchi, and S. Succi, Modeling pattern formation in soft flowing crystals, *Phys. Rev. Fluids* **4**, 072201(R) (2019).
- [39] A. Montessori, A. Tiribocchi, M. Bogdan, F. Bonaccorso, M. Lauricella, J. Guzowski, and S. Succi, Translocation dynamics of high-internal phase double emulsions in narrow channels, *Langmuir* **37**, 9026 (2021).
- [40] P. Marmottant and J. P. Raven, Microfluidics with foams, *Soft Matter* **5**, 3385 (2009).
- [41] J. P. Raven and P. Marmottant, Microfluidic Crystals: Dynamic Interplay Between Rearrangement Waves and Flow, *Phys. Rev. Lett.* **102**, 084501 (2009).
- [42] D. Y. C. Chan, E. Klaseboer, and R. Manica, Film drainage and coalescence between deformable drops and bubbles, *Soft Matter* **7**, 2235 (2011).
- [43] H. A. Stone and L. G. Leal, Breakup of concentric double emulsion droplets in linear flows, *J. Fluid. Mech.* **211**, 123 (1990).
- [44] K. A. Smith, J. M. Ottino, and M. Olvera de la Cruz, Encapsulated Drop Breakup in Shear Flow, *Phys. Rev. Lett.* **93**, 204501 (2004).
- [45] S. H. Kim, J. W. Kim, J. C. Cho, and D. A. Weitz, Double-emulsion drops with ultra-thin shells for capsule templates, *Lab Chip* **11**, 3162 (2011).
- [46] H. Chen, J. Li, H. C. Shum, H. A. Stone, and D. A. Weitz, Breakup of double emulsions in constrictions, *Soft Matter* **7**, 2345 (2011).
- [47] A. Sauret and H. C. Shum, Forced generation of simple and double emulsions in all-aqueous systems, *Appl. Phys. Lett.* **100**, 154106 (2012).
- [48] S. Succi, *The Lattice Boltzmann Equation: For Complex States of Flowing Matter* (Oxford University Press, Oxford, 2018).
- [49] G. Coupier, A. Farutin, C. Minetti, T. Podgorski, and C. Misbah, Shape Diagram of Vesicles in Poiseuille Flow, *Phys. Rev. Lett.* **108**, 178106 (2012).
- [50] C. Zhou, P. Yue, and J. J. Feng, Deformation of a compound drop through a contraction in a pressure-driven pipe flow, *Int. J. Multiphase Flow* **34**, 102 (2008).
- [51] D. Abreu, M. Levant, V. Steinberg, and U. Seifert, Fluid vesicles in flow, *Adv. Colloid Interface Sci.* **208**, 129 (2014).
- [52] J. Wang, X. Li, X. Wang, and J. Guan, Possible oriented transition of multiple-emulsion globules with asymmetric internal structures in a microfluidic constriction, *Phys. Rev. E* **89**, 052302 (2014).
- [53] A. Pommella, D. Donnarumma, S. Caserta, and S. Guido, Dynamic behaviour of multilamellar vesicles under poiseuille flow, *Soft Matter* **13**, 6304 (2017).
- [54] Z. Che, Y. F. Yap, and T. Wang, Flow structure of compound droplets moving in microchannels, *Phys. Fluids* **30**, 012114 (2018).
- [55] N. Wang, C. Semperebon, H. Liu, C. Zhang, and H. Kusumaatmaja, Modelling double emulsion formation in planar flow-focusing microchannels, *J. Fluid Mech.* **895**, A22 (2020).
- [56] G. Pontrelli, E. J. Carr, A. Tiribocchi, and S. Succi, Modeling drug delivery from multiple emulsions, *Phys. Rev. E* **102**, 023114 (2020).
- [57] J. Tao, X. Song, J. Liu, and J. Wang, Microfluidic rheology of the multiple-emulsion globule transiting in a contraction tube through a boundary element method, *Chem. Eng. Sci.* **97**, 328 (2013).
- [58] A. Tiribocchi, A. Montessori, M. Lauricella, F. Bonaccorso, S. Succi, S. Aime, M. Milani, and D. A. Weitz, The vortex-driven dynamics of droplets within droplets, *Nat. Commun.* **12**, 82 (2021).
- [59] I. S. Aranson, *Physical Models of Cell Motility* (Springer International Publishing, Switzerland, 2016).
- [60] M. Foglino, A. N. Morozov, O. Henrich, and D. Marenduzzo, Flow of Deformable Droplets: Discontinuous Shear Thinning and Velocity Oscillations, *Phys. Rev. Lett.* **119**, 208002 (2017).
- [61] A. Tiribocchi, A. Montessori, S. Aime, M. Milani, M. Lauricella, S. Succi, and D. Weitz, Novel nonequilibrium steady states in multiple emulsions, *Phys. Fluids* **32**, 017102 (2020).
- [62] A. Tiribocchi, A. Montessori, F. Bonaccorso, M. Lauricella, and S. Succi, Concentrated phase emulsion with multicore morphology under shear: A numerical study, *Phys. Rev. Fluids* **5**, 113606 (2020).
- [63] A. Tiribocchi, A. Montessori, M. Bonaccorso, F. Lauricella, and S. Succi, Shear dynamics of polydisperse double emulsions, *Phys. Fluids* **33**, 047105 (2021).
- [64] S. R. De Groot and P. Mazur, *Non-Equilibrium Thermodynamics* (Dover, New York, 1984).

- [65] L. D. Landau and E. M. Lifshits, *Fluid Mechanics*, 2nd ed. (Butterworth-Heinemann, Oxford, 1987).
- [66] T. Krüger, H. Kusumaatmaja, A. Kuzmin, O. Shardt, G. Silva, and E. M. Viggien, *The Lattice Boltzmann Method* (Springer International Publishing, Switzerland, 2017).
- [67] V. M. Kendon, M. E. Cates, I. Pagonabarraga, J. C. Desplat, and P. Blandon, Inertial effects in three-dimensional spinodal decomposition of a symmetric binary fluid mixture: A lattice boltzmann study, *J. Fluid. Mech.* **440**, 147 (2001).
- [68] M. C. Sukop and D. T. Thorne, *Lattice Boltzmann Modeling: An Introduction for Geoscientists and Engineers* (Springer International Publishing, Switzerland, 2006).
- [69] A. Montessori, M. Lauricella, N. Tirelli, and S. Succi, Mesoscale modelling of near-contact interactions for complex flowing interfaces, *J. Fluid. Mech.* **872**, 327 (2019).
- [70] A. Tiribocchi, N. Stella, G. Gonnella, and A. Lamura, Hybrid lattice Boltzmann model for binary fluid mixtures, *Phys. Rev. E* **80**, 026701 (2009).
- [71] L. N. Carenza, G. Gonnella, A. Lamura, G. Negro, and A. Tiribocchi, Lattice boltzmann methods and active fluids, *Eur. Phys. J. E* **42**, 81 (2019).
- [72] F. Bonelli, L. N. Carenza, G. Gonnella, D. Marenduzzo, E. Orlandini, and A. Tiribocchi, Lamellar ordering, droplet formation and phase inversion in exotic active emulsions, *Sci. Rep.* **9**, 2801 (2019).
- [73] G. Negro, L. N. Carenza, A. Lamura, A. Tiribocchi, and G. Gonnella, Rheology of active polar emulsions: From linear to unidirectional and inviscid flow, and intermittent viscosity, *Soft Matter* **15**, 8251 (2019).
- [74] See Supplemental Material at <http://link.aps.org/supplemental/10.1103/PhysRevE.104.065112> for movies showing the dynamics of multicore emulsions under Poiseuille flow.
- [75] J. Park and P. D. Anderson, A ternary model for double-emulsion formation in a capillary microfluidic device, *Lab Chip* **12**, 2672 (2012).
- [76] J. Guzowski and P. Garstecki, Droplet Clusters: Exploring the Phase Space of Soft Mesoscale Atoms, *Phys. Rev. Lett.* **114**, 188302 (2015).
- [77] M. Lulli, R. Benzi, and M. Sbragaglia, Metastability at the Yield-Stress Transition in Soft Glasses, *Phys. Rev. X* **8**, 021031 (2018).